CHAPTER 5

TURBULENT SHEAR FLOWS IN A STRATIFIED FLUID

The theme of this chapter will be a more detailed discussion of various kinds of turbulent shear flows, which are (at least at the beginning of the period of interest) well past the state of marginal stability. Some knowledge of the properties of a turbulent shear flow in a homogeneous fluid must be assumed (see, for example, Townsend 1956), and we consider here the additional effects introduced by the presence of density gradients. Turbulent flows in which gravity plays an essential role in driving the mean motion (e.g. turbulent gravity currents) will be treated separately in chapter 6.

These flows will be discussed against the background of the classification introduced in §4.3.1, emphasizing the turbulent features, but also referring to the wave aspects when necessary. We consider first a shear flow near a horizontal boundary, and the effect of a vertical density gradient on the velocity and density profiles, and on the rates of transport. Next we discuss the few theoretical results which are available to describe 'boundary' and 'interior' turbulence in stratified shear flows. Finally, we present and discuss laboratory and larger scale observations which can be used to test these ideas.

5.1. Velocity and density profiles near a horizontal boundary

The most important example of a shear flow near a boundary is the wind near the ground, in a shallow enough layer for the effects of the earth's rotation to be ignored. (The meaning of this limitation will be made clearer in §9.2.4.) Many of the results described below have been developed in the meteorological context (with high Reynolds number flows in mind), and a good summary is given by Priestley

(1959). We begin with a brief description of flows of uniform density before discussing the changes introduced by stratification.

5.1.1. *The logarithmic boundary layer*

Consider a semi-infinite fluid of density ρ, bounded by a horizontal plane which is being moved horizontally at such a rate that it applies a shear stress τ to the fluid near it. In the absence of a pressure gradient, τ must remain constant with height z above the plane, and at large times this produces a steady (in the mean) distribution of velocity $u(z)$ characteristic of a 'constant stress layer'. This idealized model also gives a good description of the flow close to the wall of a pipe or channel, and in the lowest few tens of metres of the atmospheric boundary layer (where the stress has changed little from its value at the boundary).

The velocity gradient responsible for maintaining this stress can be deduced by dimensional arguments. Except very close to the wall (where viscosity may be relevant), it is assumed to be a function of z, τ and ρ alone, so that

$$\frac{\mathrm{d}u}{\mathrm{d}z} = \left(\frac{\tau}{\rho}\right)^{\frac{1}{2}} \Big/ kz \equiv u_*/kz. \tag{5.1.1}$$

Here u_* is called the 'friction velocity', and k is a universal constant (von Kármán's constant, with an experimentally determined value of approximately $k = 0.41$). Integrating (5.1.1) gives

$$u = \frac{u_*}{k}(\ln z + c) \tag{5.1.2}$$

the well known logarithmic profile. The constant of integration c depends on conditions right at the surface, and changes in its value imply the addition of a uniform velocity to the whole flow with no change in its internal structure (see fig. 5.1).

When the boundary is aerodynamically smooth the stress is transmitted by viscosity; there is a viscous sublayer whose thickness is of order $\delta \sim \nu/u_*$ and in which the velocity varies linearly, like $u_*^2 z/\nu$. Matching this to (5.1.2) gives (with axes fixed in the boundary)

$$u = \frac{u_*}{k}\left(\ln \frac{u_* z}{\nu} + c_1\right), \tag{5.1.3}$$

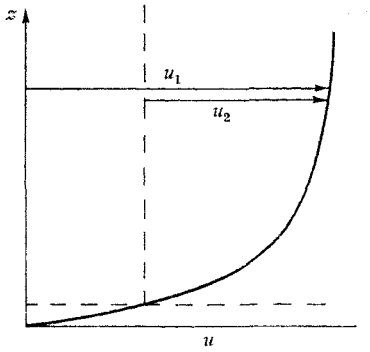

Fig. 5.1. Sketch of the velocity profile in turbulent flow past a solid plane, showing the effect of changing the boundary condition.

where c_1 is now a universal constant with an experimentally determined value of about 2.4 (see Prandtl 1952, p. 126). At an aerodynamically rough boundary the individual roughness elements have heights greater than δ; ν therefore becomes irrelevant because the stress is transmitted by pressure forces in the wakes of the roughness elements (cf. §4.3.2). The velocity profile is now

$$u = \frac{u_*}{k} \ln \frac{z}{z_0}, \tag{5.1.4}$$

where z_0, called the roughness length, is related to the geometry of the boundary.

Using (5.1.1) one can also evaluate the rate of production of mechanical energy per unit mass ϵ say (which in steady conditions, and when there is no flux of energy into or out of the region of interest, is also the rate of dissipation)

$$\epsilon = u_*^2 \frac{\mathrm{d}u}{\mathrm{d}z} = \frac{u_*^3}{kz}, \tag{5.1.5}$$

and define an eddy viscosity or vertical transport coefficient for momentum

$$K_\mathrm{M} \equiv \frac{\tau}{\rho} \Big/ \frac{\mathrm{d}u}{\mathrm{d}z} \tag{5.1.6}$$

which is equal to ku_*z for the logarithmic profile (5.1.4). The relation between the flux and the gradient of a passive tracer (such as

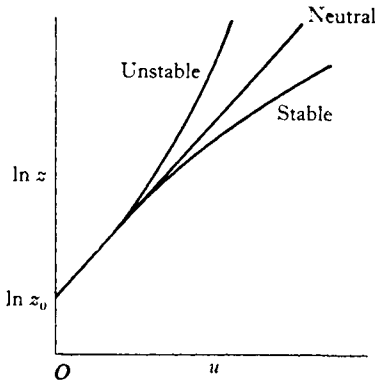

Fig. 5.2. The effect of a stable or unstable environment on turbulent velocity profiles.

a small amount of heat or moisture) is predicted to good accuracy by assuming that the turbulent diffusivities (say K_H for heat) are the same as K_M, an idea which is called 'Reynolds analogy' (see § 5.1.3). When the buoyancy associated with these properties becomes larger, however, the transfer mechanism itself is affected, the profiles change, and a separate discussion is needed. We will still assume initially that the boundary stress is dominant, i.e. that we are dealing with case (*a*) of fig. 4.19.

5.1.2. *The effect of a buoyancy flux*

The extra parameter of dynamical significance is the buoyancy flux, defined by

$$B = -g\overline{\rho' w'}/\bar{\rho}, \tag{5.1.7}$$

where ρ' and w' are the fluctuations of density and vertical velocity and the bar denotes an average (over a horizontal area, or over time at a fixed point). When one is dealing with a heat flux H (positive upwards) in a gas, then $B = (g/\bar{\theta})(H/C_p\rho)$, where C_p is the specific heat and $\bar{\theta}$ the absolute temperature. For the purposes of discussion B, as well as u_*, is usually taken to be constant with height, but this can only be a good approximation in a layer of limited depth (see § 7.3.3). Transports by any other mechanism (such as heat radiation) are neglected here.

Following Monin and Obukov (1954), we now show how the properties of the flow are determined when u_* and B are taken as the fundamental parameters. From these can be formed the 'Monin–Obukov length'

$$L = \frac{\bar{\rho} u_*^3}{kg\overline{\rho' w'}} = \frac{-u_*^3}{kgH/C_p\rho\bar{\theta}} = \frac{-u_*^3}{kB}, \qquad (5.1.8)$$

a scaling parameter for the flow which is negative in unstable conditions (e.g. heating from below) and positive in stable conditions. All dimensionless variables must now be functions of z/L. Equation (5.1.1) is replaced by

$$\frac{kz}{u_*}\frac{\mathrm{d}u}{\mathrm{d}z} = \phi_{\mathrm{M}}\left(\frac{z}{L}\right) \qquad (5.1.9)$$

(which implies that $K_{\mathrm{M}} = ku_* z/\phi_{\mathrm{M}}$), and the relations obtained by integrating (5.1.1) must be modified correspondingly.

The function ϕ_{M} has two basic forms, one in stable and the other in unstable conditions, and the description in terms of these universal functions receives support from measurements in the atmosphere (see fig. 5.3). Any further theoretical discussion, however, requires special assumptions about ϕ_{M}, going beyond the simple dimensional argument. If ϕ_{M} is expressed as a power series in z/L, and only the linear term is retained ($\phi_{\mathrm{M}} = 1 + \alpha z/L$) then (5.1.9) leads to

$$u = \frac{u_*}{k}\left[\ln\frac{z}{z_0} + \alpha\frac{z}{L}\right], \qquad (5.1.10)$$

i.e. to a log-linear profile, where α has a value of about five (see Webb 1970). Such deviations from the logarithmic profile in opposite senses in stable and unstable conditions are observed (see fig. 5.2), the velocity increasing less rapidly than $\ln z$ in an unstable environment (z/L negative) because of the increased vertical mixing caused by convection.

In the same way a non-dimensional density (or potential temperature) gradient can be defined, such that

$$\frac{ku_* z}{\overline{\rho' w'}}\frac{\mathrm{d}\rho}{\mathrm{d}z} = \frac{ku_* z}{\overline{\theta' w'}}\frac{\mathrm{d}\theta}{\mathrm{d}z} = \frac{kz}{T_*}\frac{\mathrm{d}\theta}{\mathrm{d}z} = \phi_{\mathrm{H}}\left(\frac{z}{L}\right), \qquad (5.1.11)$$

where $T_* = \overline{\theta' w'}/u_*$ is a convenient temperature scale. Another

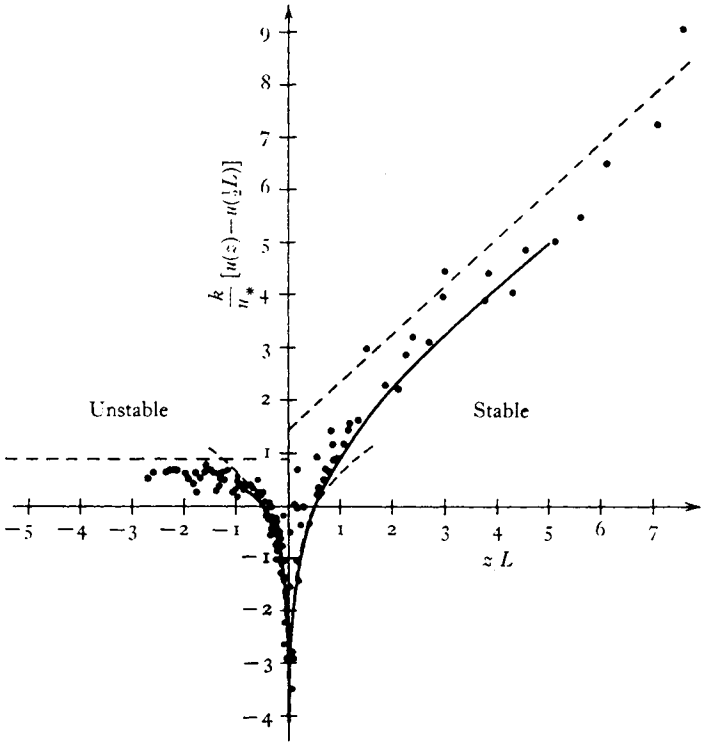

Fig. 5.3. Plot of experimental data in the finite difference form used by Monin and Obukov, showing the behaviour in stable and unstable conditions. (From Monin 1962*a*.)

function ϕ_I can be defined similarly for each transferred property, such as water vapour or a pollutant, and the use of 'Reynolds analogy' implies that the ϕs and hence the 'eddy transport coefficients' are equal. This seems to be a good assumption for heat, water vapour and dynamically neutral pollutants, but the experimental evidence described later suggests that momentum behaves differently; both ϕ_M^{-1} and K_H/K_M decrease as z/L increases (i.e. as the density gradient becomes more stable).

The gradient Richardson number Ri (1.4.3) can be used in this context as an alternative but slightly less convenient stability parameter. Of more direct physical significance is the flux Richardson number Rf, the ratio of the rate of removal of energy by buoyancy

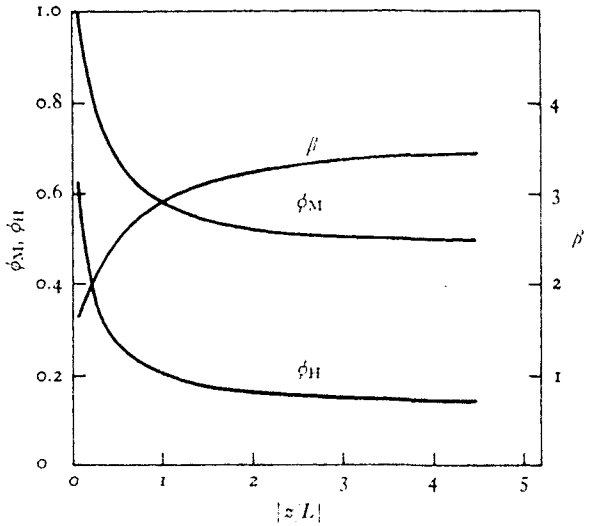

Fig. 5.4. The forms of the non-dimensional profile functions, and their ratio, derived from more recent analyses of observations in unstable conditions. (From Charnock 1967.)

forces to its production by the shear, which can be expressed in several equivalent ways:

$$Rf = \frac{K_H}{K_M} Ri = \frac{g\overline{\rho' w'}}{\bar{\rho} u_*^2 \, \mathrm{d}u/\mathrm{d}z} = \frac{K_M}{k u_* L}. \qquad (5.1.12)$$

Thus near the limit of zero density gradient, where K_M and K_H are nearly equal, $Ri \approx Rf = z/L$.

In general Ri, Rf and K_H/K_M, as well as the non-dimensional profiles, are more complicated functions of z/L, whose forms are now known empirically from the observations in the lower atmosphere. Several other limiting cases are treated below.

5.1.3. *Forced and free convection*

It will be useful to digress from the main theme of this chapter to discuss briefly the effect of an unstable buoyancy flux on a turbulent shear flow (although convection problems where turbulence due to the mean flow is entirely absent are left until chapter 7). When $|z/L|$ is sufficiently small, the generation of turbulence by the shear

dominates over generation by buoyancy; the deviation from neutral conditions is small, and the process of transfer of buoyancy (heat) is called 'forced convection'. The buoyancy flux can be calculated by putting $K_H = K_M = k^2z^2(\mathrm{d}u/\mathrm{d}z)$; it follows that

$$\overline{\rho' w'} = K_H \frac{\mathrm{d}\rho}{\mathrm{d}z} = k^2 z^2 \left(\frac{\mathrm{d}u}{\mathrm{d}z}\right)\left(\frac{\mathrm{d}\rho}{\mathrm{d}z}\right). \tag{5.1.13}$$

When this flux as well as u_* is constant with height, the density gradient is proportional to z^{-1} and the profile is again logarithmic.

'Free convection', on the other hand, occurs at large negative values of z/L, in a range where the contributions to the vertical transfer of momentum and (say) heat by mechanical turbulence can be neglected compared to those carried by convection. This does *not* mean that the mechanically generated energy itself is negligible – it may be comparable with that generated by buoyancy, and indeed over a smooth boundary the existence of the shear flow is implied if molecular conduction near the boundary is not to become important (see fig. 5.5, and also Townsend (1962), which is discussed in §7.1.3). It does mean that u_* and L are no longer relevant parameters, so that the density gradient or the dynamically more significant quantity $(g/\rho)(\mathrm{d}\rho/\mathrm{d}z)$ (cf. N^2; but the gradient is now unstable) should depend on height z and $B = -g\overline{\rho' w'}/\bar{\rho}$. (Over a rough boundary z_0 can in principle also be relevant.) A dimensional argument shows that the form of the relation between them must be

$$B\left(\frac{g}{\rho}\frac{\mathrm{d}\rho}{\mathrm{d}z}\right)^{-\frac{2}{3}} z^{-2} = H_*, \tag{5.1.14}$$

where H_* is the 'non-dimensional buoyancy flux', a constant in free convection with an experimental value close to unity. Rewriting (5.1.14) in the notation appropriate for a heat flux one obtains

$$\left.\begin{aligned} -\frac{g}{\bar{\theta}}\frac{\mathrm{d}\theta}{\mathrm{d}z} &= H_*^{-\frac{2}{3}}\left(\frac{gH}{\bar{\theta}C_p\rho}\right)^{\frac{2}{3}} z^{-\frac{4}{3}}, \\ -\frac{\mathrm{d}\theta}{\mathrm{d}z} &= H_*^{-\frac{2}{3}}\left(\frac{H}{C_p\rho}\right)^{\frac{2}{3}}\left(\frac{g}{\bar{\theta}}\right)^{-\frac{1}{3}} z^{-\frac{4}{3}}. \end{aligned}\right\} \tag{5.1.15}$$

(The parameter $g/\bar{\theta}$ has sometimes been regarded as a separate entity, but it is undesirable and sometimes misleading to do this.)

Integrating (5.1.15) with $\overline{\theta}$ and ρ regarded as fixed gives $\theta \propto z^{-\frac{1}{3}}$ (but note that ln θ should replace θ when the temperature varies markedly through the range of interest). With the assumption of similar profiles for temperature and velocity, it follows for large negative z/L that

$$\frac{u}{u_*} \propto \left(-\frac{z}{L}\right)^{-\frac{1}{3}}. \tag{5.1.16}$$

Both K_H and K_M become independent of u_* in the limit of free convection (and proportional to $z^{\frac{4}{3}}$), so $K_H/K_M = \beta$ approaches a constant and $\phi_M \propto Rf^{-\frac{1}{4}}$. These conclusions are supported by the observed forms of β, ϕ_H and ϕ_M in very unstable conditions, as summarized in fig. 5.4 (after Charnock (1967) who used a set of observations reported by Dyer (1965)).

The non-dimensional heat flux defined by (5.1.14) can also be evaluated for *forced* convection. In that case it follows from (5.1.13) that H_* is not constant, but a function of the stability parameters:

$$H_{*\text{forced}} = k^2|Ri|^{-\frac{1}{2}} = k^2\left(-\frac{z}{L}\right)^{-\frac{1}{2}}. \tag{5.1.17}$$

These predictions about H_* are again supported by observations, which show that there is a transition from the $|Ri|^{-\frac{1}{2}}$ dependence of H_* to the constant value characteristic of free convection at a very small value of $|z/L|$, about 0.03. (See fig. 5.5.) At very large negative Ri, H_* tends to rise again over a smooth boundary as molecular effects make another lengthscale relevant near the boundary (Townsend 1962).

It is convenient for some purposes to be able to write down an explicit expression for ϕ_M which has the right limiting behaviour in extreme conditions and represents the observations reasonably well over the whole range. Ellison (1957) suggested the form

$$\frac{du}{dz} = \frac{u_*}{kz}(1 - \gamma Rf)^{-\frac{1}{4}} \tag{5.1.18}$$

which can be rewritten using (5.1.9) and (5.1.12) as

$$\phi_M{}^4 - \gamma\frac{z}{L}\phi_M{}^3 = 1, \tag{5.1.18a}$$

where γ is a constant, experimentally about 14. This has been taken

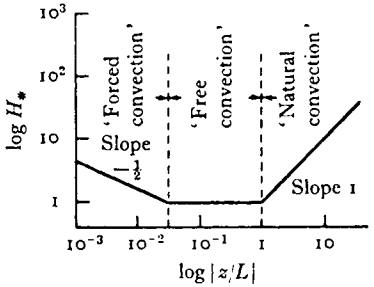

Fig. 5.5. Variation of the non-dimensional buoyancy flux H_* with z/L over the whole unstable range (schematic). (After Townsend 1962.)

up (and derived again independently) by others and widely used, but its status as an interpolation formula (rather than a strict theoretical deduction) tends to be forgotten. Neither this nor other formulae derived by more mechanistic arguments has been found satisfactory over the whole range of stability conditions, though it has been applied even in stable conditions by using a different value of γ in that range.

5.1.4. *Constant-flux layers in stable stratification*

Let us now return to the case of more immediate concern here, a stable density gradient produced (for example) by a downward (negative) buoyancy flux. In moderately stable conditions the observed velocity and density profiles are nearly similar to one another, and can again be described by the log-linear form (5.1.10) with nearly the same value of α (Webb 1970).

Using (5.1.12) we find

$$\phi_M = 1 + \alpha \frac{z}{L} = (1 - \alpha Rf)^{-1} \qquad (5.1.19)$$

which implies that Rf has a maximum (critical) value near $Rf = \alpha^{-1}$ ($\approx \frac{1}{5}$ experimentally), at which ϕ_M becomes very large and hence K_M small. From its definition, Rf cannot exceed unity, but here we have an indication (which is given further support in §5.2.3) that the value of Rf at which the turbulent transport is substantially altered can be much less than one. That is, most of the energy is always dissipated by viscosity, and only a small fraction by working against gravity.

In very stable conditions, the argument based on (5.1.19) will not be valid, but in the limit $z/L \to \infty$, Ellison (1957) has suggested that the *linear* dependence of ϕ_M on z/L is preserved. This result can be approached by a more direct dimensional argument, based on the following physical reasoning which is closely related to the views expressed by Stewart (1969). In a very stable gradient, the mixing motions must be so strongly damped that the vertical excursions of fluid parcels will be limited entirely by the work done against gravity. (This is case (*c*), referred to in §4.3.1.) All levels in the interior of the fluid must behave in the same way and will not be directly influenced by the boundaries, because mixing can occur only with adjacent fluid and cannot now extend right to the solid wall. (There will still be an indirect effect of the boundaries, where the assumed constant stress and buoyancy flux are applied; the extent to which it is *consistent* to retain all these assumptions will be taken up again in chapter 10.) It follows that any distance z (from a wall) becomes irrelevant in very stable conditions; L defined by (5.1.8) is the only lengthscale, and the velocity and density gradient must be determined by u_* and $B = -g\overline{\rho' w'}/\bar{\rho}$ alone. Thus on dimensional grounds

$$\frac{\mathrm{d}u}{\mathrm{d}z} = k_1 \frac{-B}{u_*^2} = k_1 \frac{u_*}{L} = \frac{k_1}{k_2} N \tag{5.1.20}$$

and

$$N^2 = -\frac{g}{\rho}\frac{\mathrm{d}\rho}{\mathrm{d}z} = k_2^2 \frac{B^2}{u_*^4} = k_2^2 \frac{u_*^2}{L^2}, \tag{5.1.21}$$

where k_1 and k_2 are (as yet undetermined) constants. Both profiles are linear, as stated above, and the flow is in a kind of equilibrium, self-regulated state. This result receives support from observations in the atmosphere in very stable conditions, such as above Antarctic snowfields, though in such cases it is hard to justify the constant heat flux assumption. (For a discussion of the observations in this stability range, see Oke 1970 and Webb 1970.) The other quantities defined previously will in this stable limit also attain internally regulated values, which can be expressed in terms of u_*, B, k_1, k_2. The flux Richardson number $Rf = k_1^{-1}$, and is thus related to the fluxes and the velocity profile alone. We find also that

$$K_M = \frac{u_*^4}{k_1 B} = \frac{u_* L}{k_1}, \quad K_H = \frac{u_*^4}{k_2^2 B} = \frac{u_* L}{k_2^2} \tag{5.1.22}$$

so that
$$\frac{K_H}{K_M} = \frac{k_1}{k_2^2}, \quad Ri = k_2^2/k_1^2 \tag{5.1.23}$$

and the gradient Ri also has a constant ('equilibrium') value in a turbulent constant flux layer with a stable gradient.

It must be emphasized that this last result will only hold in practice under rather special circumstances, when the external conditions exactly match the internally regulated gradients. An apparently contradictory result has been suggested for more stable flows (with large overall Richardson number Ri_0, based on the whole depth), and it will be helpful to make the difference clear immediately. The latter case corresponds to (*g*) of fig. 4.19, in which the turbulence is so strongly damped that the motion is more appropriately described as a field of random, intermittently breaking gravity waves. While it may be possible to define a local gradient Ri through the individual turbulent patches which will have the same significance as (5.1.23), any measured, time averaged value for the fluid as a whole will be more nearly akin to Ri_0. A critical value of a flux Richardson number (which is always imposed by energy considerations) does not, however, imply any limit on this 'average gradient Richardson number'.

Since the internal wave motions can readily transfer momentum through the action of pressure forces, but relatively little heat or matter even when the waves 'break', the ratio K_H/K_M can become small. Thus both transfer coefficients remain larger than the molecular values and some transfer persists to large values of 'average gradient Richardson number', while still satisfying (5.1.12), with $Rf < 1$. (See also §§5.2.3 and 10.2.2.) Laboratory results consistent with the 'equilibrium' conditions are discussed in §6.2.4, and measurements made in a large scale flow of the second kind are described in §5.3.3.

5.2. Theories of turbulence in a stratified shear flow

Compared to the case of uniform density, little is known about the properties of turbulence in a stratified fluid. In this section we outline various theories which have been proposed to study the fluctuating motions themselves, their maintenance, and the diffusion they

produce. Most of these invoke rather more explicit assumptions about the effect of stratification on the structure of the flow, but we begin with the results which follow from a simple extension of the similarity arguments used in § 5.1. (See Lumley and Panofsky 1964.)

5.2.1. *Similarity theories of turbulence and diffusion*

Dimensional reasoning can be applied to the fluctuating quantities in just the same way as they were to the form of the mean profiles. Again u_*, B and z are the governing parameters, and variables like the variance of the vertical velocity fluctuations $\sigma_w = \langle w'^2 \rangle^{\frac{1}{2}}$ or of the buoyancy fluctuations $\sigma_\rho = g\langle \rho'^2 \rangle^{\frac{1}{2}}/\rho$ can be expressed as

$$\left.\begin{aligned} \sigma_w &= u_* f_1\left(\frac{z}{L}\right) \\ \text{and} \qquad \sigma_\rho &= \frac{B}{u_*} f_2\left(\frac{z}{L}\right). \end{aligned}\right\} \tag{5.2.1}$$

Here f_1 and f_2 are universal functions which can be related to ϕ_M and ϕ_H describing the profiles, and are constants in neutral conditions. In free convection (when u_* no longer enters explicitly)

$$\sigma_w \propto B^{\frac{1}{3}} z^{\frac{1}{3}} \tag{5.2.2}$$

and the velocity fluctuations increase with height; similarly

$$\sigma_\rho \propto B^{\frac{2}{3}} z^{-\frac{1}{3}}. \tag{5.2.3}$$

In stable conditions, the stratification is more important at larger z, and σ_w is a decreasing function of height. The forms of these functions (and related quantities such as 'gustiness' and the deviation of the wind direction from the mean) have been calculated using extensions of the log-linear theory and the interpolation formula (5.1.19), and agreement between theory and observation is reasonably good. The variation with stability of two of them is shown in fig. 5.6, after Monin (1962*a*). The variance of the horizontal velocity σ_u is relatively poorly predicted by similarity theory, since this is strongly influenced by larger scale motions, not just by the local properties.

The diffusion of a neutrally buoyant pollutant (such as smoke) in

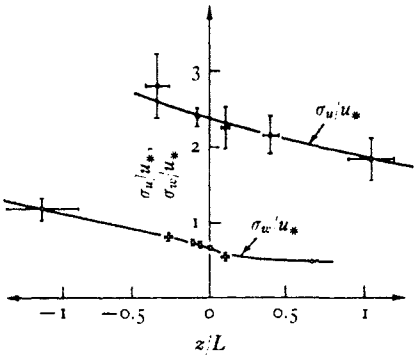

Fig. 5.6. The variances of vertical and horizontal velocity in the atmosphere near the ground, as functions of stability. (From Monin 1962*a*.)

a given stratified shear flow can also be approached by similar dimensional arguments. The Lagrangian vertical velocity

$$\mathrm{d}\bar{z}(t)/\mathrm{d}t = w_*,$$

say, following a typical particle released from the boundary into a constant stress layer, will be (Monin 1959, Ellison 1959)

$$w_* = bu_* f_3(z/L), \tag{5.2.4}$$

where f_3 is another universal function and b is a constant. The mean horizontal velocity is given by a relation like (5.1.10) so that the slope of the mean top of the smoke plume, $\mathrm{d}x/\mathrm{d}z = u/w_*$, will be a function of z/L (i.e. of stability) but not of mean velocity. In neutral conditions, the rate of spread becomes nearly linear some distance above the ground where u is changing slowly, and the concentration at the ground is inversely proportional to x. This result differs from the parabolic spread predicted by ordinary diffusion in a constant cross-stream flow, since it takes properly into account the increasing scale of the turbulence at greater heights. In unstable conditions the rate of spread increases, and in stable conditions it decreases (see fig. 5.7). A good summary of the predictions of similarity theory and the comparison with observations has been given by Klug (1968).

5.2.2. *The spectrum of nearly inertial turbulence*

Something should be said next about an idea which seemed promising when it was first introduced, but which is of limited

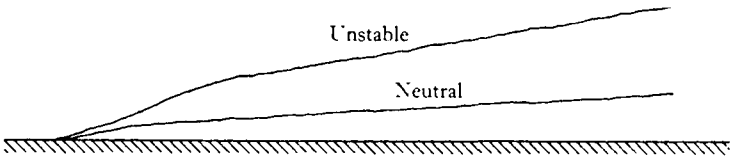

Fig. 5.7. The mean spread of the top of smoke plumes rising from the ground in neutral and unstable conditions. (After Monin 1959.)

practical significance for reasons which will become apparent. It is an extension of Kolmogorov's theory of 'local similarity' which is based on the idea of an energy cascade from small to large wavenumbers in a turbulent flow, and gives information about scales of motion much smaller than those of length scale l_1 and velocity scale u_1 at which energy is put into a constant density flow at high Reynolds number. A thorough discussion of this theory would take us too far afield here, and only the final result will be quoted; reference should be made to Batchelor (1953*b*, p. 114), Monin (1962*b*) and Phillips (1966*a*, p. 213) for the background to this problem.

Kolmogorov's second hypothesis leads to a description of the form of the spectrum, or the energy density function $E(k)$, in an 'inertial subrange' where viscous effects are unimportant. In this range $E(k)$ is determined entirely by two parameters, the magnitude of the wavenumber k and the rate of transfer of energy through the spectrum. The latter can be equated either to the rate of decay of the energy-containing eddies (which is of order u_1^3/l_1, cf. (5.2.15)) or to the eventual energy dissipation per unit mass ϵ_0 by the smallest eddies. The function $E(k)$ is related to the kinetic energy per unit mass $q^2 = \overline{u'^2} + \overline{v'^2} + \overline{w'^2}$ by

$$\tfrac{1}{2}q^2 = \int_0^\infty E(k)\,\mathrm{d}k, \tag{5.2.5}$$

and the form predicted using a dimensional argument is

$$E(k) = A\epsilon_0^{\frac{2}{3}}k^{-\frac{5}{3}}. \tag{5.2.6}$$

This prediction has received firm support from experiments made in a tidal estuary by Grant, Stewart and Moilliet (1962), whose measurements also give a value for the numerical constant ($A \approx 1.5$). A '$-\frac{5}{3}$ power law' has been used to describe a wide variety of geophysical data, but (5.2.6) has quite unreasonably been elevated

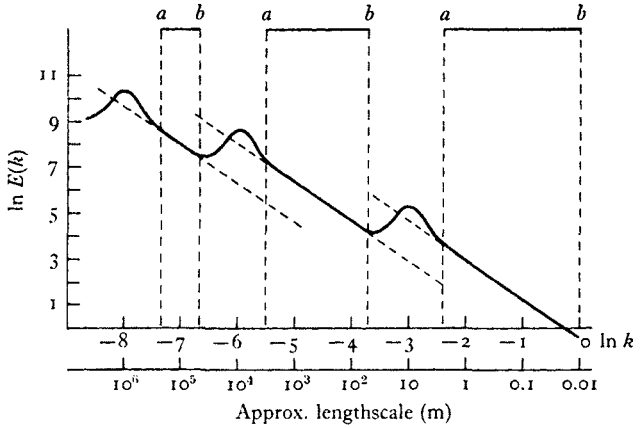

Fig. 5.8. Schematic diagram of the distribution of energy in the ocean as a function of wavenumber. Ranges a–b are those in which a '$\frac{5}{3}$ power law' may be applicable, though between them there is an energy input. (From Ozmidov 1965*a*.)

to the status of a general principle, without paying enough attention to the assumptions on which it is based (which include the condition that the turbulence should be isotropic in this range).

The arguments leading to (5.2.6) can break down if there is any substantial transfer of energy directly into or out of the 'inertial subrange'. Convective motions in the atmosphere can add energy at intermediate scales, for instance; but Ozmidov (1965*a*) has suggested that if this input is confined to a small range of wavenumbers, the $-\frac{5}{3}$ power law may still apply for values of k on either side of this. There will then be a jump in the E, k curve corresponding to each input (see fig. 5.8), but it can continue with the same slope at a higher level corresponding to the increased value of ϵ_0, the new rate of energy supply to higher wavenumbers.

Of more interest here is the possibility that, in a stratified fluid, there could be a systematic removal of turbulent kinetic energy over a range of wavenumbers, by working against buoyancy forces. This could only happen in a region of fully turbulent fluid (such as one of the turbulent patches referred to at the end of §5.1.4) in which the departure from neutral conditions is small, and it is still reasonable to think in terms of a cascade of energy through the spectrum. Regions where the Richardson number is large are

therefore excluded; then the motions are more appropriately described as a set of weakly interacting waves (cf. §2.4.3), which can transfer energy selectively to remote wavenumbers. Moreover, it will become clear below that a significant buoyancy effect of the kind envisaged is only possible where energy is injected into a region from an external source, not where it is produced by the local shear.

The smallest scales of motion will remain unaffected in stable stratification, while buoyancy forces first become important for the larger length scales. Thus the discussion of the constant-flux boundary layer (5.1.10) indicates that buoyancy forces are significant at heights comparable with and greater than L (the Monin–Obukov length). The laboratory observations of Grigg and Stewart (1963), of turbulent vortices projected through a stratified fluid, show directly that the largest scales (i.e. the mean motion) are suppressed first, leaving the smaller scale turbulence practically unchanged. These results suggest that there could be a wavenumber k_b say, replacing L^{-1} in the present problem, at which one can further divide the wavenumbers previously comprising the inertial subrange. In the 'buoyancy subrange', such that

$$l_1^{-1} \ll k < k_b \tag{5.2.7}$$

the loss of energy due to working against buoyancy can, it is argued, become comparable with that transferred. The physical parameters on which k_b can depend are ϵ_0 and N^2, and so on dimensional grounds

$$k_b = c_1 N^{\frac{3}{2}} \epsilon_0^{-\frac{1}{2}}, \tag{5.2.8}$$

where c_1 is a positive constant. An equivalent argument was used by Ozmidov (1965*b*) to determine the critical length scale at which buoyancy forces become important in the oceanic boundary layer. The corresponding maximum vertical transfer coefficient can be expressed in the form

$$K_M \propto \epsilon_0 N^{-2}. \tag{5.2.9}$$

Ozmidov also showed that in such a 'buoyancy subrange' the motion must become anisotropic because not only are the horizontal motions undamped by gravity, but some of the vertical energy is transferred to them.

Dimensional reasoning can take us a step further. In the 'buoyancy subrange', if it exists, the local rate of energy transfer

$\epsilon(k)$ through the spectrum will be much larger than the eventual dissipation rate ϵ_0, since the latter is by definition the residual rate of transfer after energy has been extracted by working against gravity at all larger scales. Thus ϵ_0 is not an important parameter in the buoyancy subrange,† and the form of the spectrum must be determined by N^2 and k, since $\epsilon(k)$ is itself a derived function. It follows that

$$E(k) = c_2 N^2 k^{-3}. \tag{5.2.10}$$

Lumley (1964) used more explicit assumptions to derive a form for the complete buoyancy-inertial subrange, but in view of the rather special conditions under which it could be applicable, this will not be pursued further here.

The form (5.2.10) has received limited support from aircraft observations of atmospheric turbulence, though there must always be some doubt whether these were indeed made within fully turbulent air, as implied by the theory. Myrup (1968), for example, flew through a stable layer at the top of a convecting surface layer (cf. §9.2.3), and found a range of k, where $E(k) \propto k^{-3}$ approximately, changing to $k^{-\frac{5}{3}}$ at higher wavenumbers, in agreement with (5.2.6) for the inertial subrange. No buoyancy subrange has been detected in laboratory experiments.

Two major criticisms can be levelled against the interpretation of such observations in terms of a buoyancy subrange. Most important, the relation (5.2.7) is rarely satisfied in the atmosphere, so that there may be no range of scales in which the underlying assumptions are properly satisfied and the buoyancy effect dominant. Secondly, measurements of the kind quoted in the preceding paragraph could include an unknown contribution from internal waves. This is perhaps a less serious objection, since in a buoyancy subrange, the distinction between the non-isotropic turbulence described above and the forced, strongly interacting internal waves referred to at the end of chapter 2 becomes blurred. In fact the form (5.2.10) is identical to the condition (2.4.9), which ensures that strong interactions will dominate over the weak, selective wave interactions.

† This is quite different from the more usual situation where there is a local balance between production and dissipation of turbulent energy, with no external source. In the latter case, viscous dissipation will dominate over the buoyancy term even in stable stratification – see §5.2.3.

Whatever words are used to describe the process, each of these pictures implies a cascade of energy through the spectrum to higher wavenumbers, and relates the form of $E(k)$ to the same two physical parameters k and N^2. The 'turbulence' description is perhaps the more helpful, because it makes clear that working against gravity, and hence wave breakdown and mixing, is a necessary part of the mechanics of a buoyancy dominated subrange.

5.2.3. *Arguments based on the governing equations*

In this section we compare several attempts to deduce the structure of turbulence in a unidirectional stratified shear flow, which apply similarity hypotheses to the dynamical equations rather than directly to the external parameters. The flow is assumed to be fully turbulent and of high Reynolds number, and no molecular diffusion effects are included here. (See §9.1.3 for a discussion of this last point.) Arguments which also take wave propagation into account explicitly will be left until the final chapter.

For simplicity, horizontal homogeneity will be assumed here, though the results will be applied later (with some reservations) to developing flows such as wakes. In the absence of advection, the equations for the turbulent kinetic energy per unit mass

$$\tfrac{1}{2}q^2 = \tfrac{1}{2}(\overline{u'^2} + \overline{v'^2} + \overline{w'^2})$$

and the mean square density fluctuation may be expressed in the forms (derived from the Navier–Stokes equations):

$$\frac{1}{2}\frac{\partial q^2}{\partial t} + \frac{1}{2}\frac{\partial \overline{q^2 w'}}{\partial z} + \overline{u'w'}\frac{\partial u}{\partial z} + \frac{1}{\bar{\rho}}\frac{\partial \overline{w'p'}}{\partial z} + \frac{g}{\bar{\rho}}\overline{\rho' w'} + \epsilon_0 = 0, \quad (5.2.11)$$

$$\frac{1}{2}\frac{\partial \overline{\rho'^2}}{\partial t} + \frac{1}{2}\frac{\partial \overline{\rho'^2 w'}}{\partial z} + \overline{\rho' w'}\frac{\partial \bar{\rho}}{\partial z} - \kappa\overline{\rho'\nabla^2\rho'} = 0. \quad (5.2.12)$$

In the steady state, and neglecting small 'diffusion' terms like $\partial(\overline{q^2 w'})/\partial z$ (or alternatively, regarding u' etc. as vertically averaged values), (5.2.11) reduces to

$$\tau\frac{\partial u}{\partial z} = -\overline{u'w'}\frac{\partial u}{\partial z} = \frac{g}{\bar{\rho}}\overline{w'\rho'} + \epsilon_0, \quad (5.2.13)$$

where the terms are respectively the production by the Reynolds stress working against the mean velocity gradient, the rate of working against buoyancy, and viscous dissipation.

By considering the equations for the separate components (see, for example, Stewart (1959)) it can be shown that the energy is put initially into the $\overline{u'^2}$ component, that in the direction of mean motion, but is redistributed by pressure fluctuations among all three turbulent velocity components. The loss to buoyancy affects only $\overline{w'^2}$ directly, whereas viscosity affects all three. Moreover, the mechanism which tends to make the turbulence isotropic is known (from experiments in flows of constant density) to be inefficient compared to the decay mechanism. Thus we can already see qualitatively how the buoyancy term, though making only a small direct contribution to the energy dissipation, can have a large effect on the turbulence. Even in a stratified fluid ϵ_0 remains the dominant term on the right hand side of (5.2.13), so that the maximum value of Rf (defined by (5.1.12)) will be much less than unity.

The corresponding equation to (5.2.13) for the density fluctuations may be written

$$\overline{w'\rho'}\frac{\partial\overline{\rho}}{\partial z}+\chi=0, \tag{5.2.14}$$

where the terms are respectively the rates of production and dissipation of mean square density fluctuations. Further progress depends on the assumptions made at this point about the forms of ϵ_0 and χ; those due to Townsend (1958) will be considered first. He supposed that results which have been used to relate ϵ_0 and χ to the large scale properties of a constant density flow (Batchelor 1953*b*, p. 102) will continue to be valid in stable stratification. Explicitly, he put

$$\epsilon_0=q^3/L_u, \quad \chi=\overline{\rho'^2}q/L_\rho \tag{5.2.15}$$

where L_u and L_ρ are characteristic integral scales which are assumed to remain in a fixed ratio even in a stratified flow. Substituting in (5.2.13) and (5.2.14) and rearranging gives

$$\overline{w'\rho'}=-k_\rho^2 L_\rho q\frac{\partial\overline{\rho}}{\partial z} \tag{5.2.16}$$

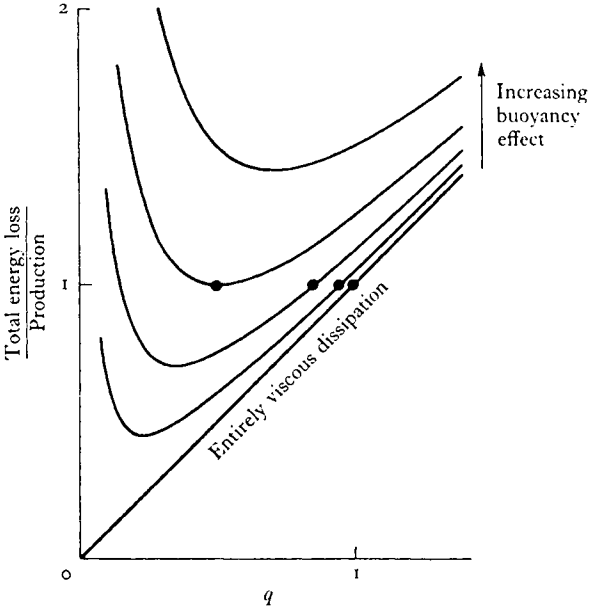

Fig. 5.9. The ratio of total energy loss to energy production in a stratified flow, as a function of the turbulent intensity for various ratios of the buoyant and viscous contributions to the energy dissipation. (From Townsend 1958.)

and
$$-\overline{u'w'}\frac{\partial u}{\partial z} = -k_u q^2 \frac{\partial u}{\partial z} = -\frac{g}{\bar{\rho}} k_\rho^2 L_\rho q \frac{\partial \bar{\rho}}{\partial z} + \frac{q^3}{L_u}, \qquad (5.2.17)$$

where
$$k_\rho^2 = \frac{(\overline{w'\rho'})^2}{q^2\overline{\rho'^2}}, \quad k_u = \frac{\overline{u'w'}}{q^2}. \qquad (5.2.18)$$

To complete the solution, Townsend also had to assume that k_ρ^2 and k_u are constants (averaged across the flow section and independent of stability) and that the velocity and density gradients are also nearly constant.

The ratio of the total energy loss to the production (the ratio of the right hand to the left hand side of (5.2.17)) is plotted in fig. 5.9 as a function of the turbulent intensity q, for several ratios of the two dissipation terms. Possible equilibrium points are marked; clearly no equilibirum intensity exists for curves whose minimum value exceeds unity, i.e. for which the assumed buoyancy contribution is too large. At each minimum, the buoyant and viscous terms are

equal on this model, and so $Rf_{\max} = \frac{1}{2}$. (This numerical value can change with different detailed assumptions, but the essential features of the model are preserved provided one of the terms on the right of (5.2.17) increases and the other decreases with increasing q.) The turbulent intensity is finite in the critical flow, and a sudden collapse of the turbulence occurs as the limit is passed.

By solving (5.2.17) for q and substituting the result in (5.2.16), Rf can be expressed in terms of gradients as

$$Rf = \frac{1}{2}\left[1 - \left(1 - 4\frac{L_\rho}{L_u}\frac{k_\rho^2}{k_u^2}Ri\right)^{\frac{1}{2}}\right]. \tag{5.2.19}$$

Thus Townsend's assumptions lead to the conclusion that the gradient Richardson number Ri will also have a critical value

$$Ri_{\text{crit}} = \frac{1}{4}\frac{L_u}{L_\rho}\frac{k_u^2}{k_\rho^2} \tag{5.2.20}$$

above which no real solutions to the balance equations are possible. This is in agreement with the simple deduction made in § 5.1.4, and it is supported also by the later theories of Monin (1965) and Ellison (1966), to which further reference is made below. No satisfactory theoretical estimate of Ri_{crit} has yet been made, but the experimental results to be discussed in § 5.3 suggest that $Ri_{\text{crit}} \approx 0.1$.

The most questionable of the assumptions made by Townsend are that k_u, and especially k_ρ, are constants independent of stability. This can certainly not remain true in the final stages of decay when the vertical motions are strongly damped, for much the same reasons as those outlined at the end of § 5.1 to show that K_{H} can become much less than K_{M}. It is also not clear how the averages are to be taken, especially in a boundary layer where such properties will be strong functions of the height.

With the constant-flux boundary layer in mind, Ellison (1957) proposed a method which avoids some of these difficulties. This was the first attempt to use simplifications of the dynamical equations to study the effect of stratification, and it still merits careful consideration, though that author has since developed a more ambitious model. He again used (5.2.13) and (5.2.14), but replaced (5.2.15) by

$$\epsilon_0 = q^2/T_2, \quad \chi = \overline{\rho'^2}/T_1, \tag{5.2.21}$$

i.e. he defined decay times T_1 and T_2 such that (in the absence of production) turbulence would begin to destroy $\overline{\rho'^2}$ and q^2 at rates T_1^{-1} and T_2^{-1}. (Compare also with the full equations (5.2.11) and (5.2.12).) Instead of deriving an expression for $\overline{w'\rho'}$ from these (which led previously to a constant k_ρ), he used an additional equation for the change in the density flux. With the same approximations as before, and introducing a separate timescale T_3 for the decay of $\overline{w'\rho'}$, this is

$$\overline{w'^2}\frac{\mathrm{d}\bar{\rho}}{\mathrm{d}z}+\frac{\overline{\rho'^2}g}{\bar{\rho}}+\frac{\overline{w'\rho'}}{T_3}=0. \tag{5.2.22}$$

The three equations involving T_1, T_2 and T_3 can be rearranged to express the ratio of eddy transport coefficients (defined by (5.1.6), and equivalently for buoyancy) in the form

$$\begin{aligned}\frac{Rf}{Ri}=\frac{K_\mathrm{H}}{K_\mathrm{M}}&=\frac{q^2\overline{w'^2}\left[1-Rf\left(1+\dfrac{q^2}{\overline{w'^2}}\dfrac{T_1}{T_2}\right)\right]}{(\overline{u'w'})^2(T_2/T_3)(1-Rf)^2}\\&=\frac{b(1-Rf/Rf_\mathrm{crit})}{(1-Rf)^2},\end{aligned} \tag{5.2.23}$$

where b is a constant. If it is supposed that $T_1\approx T_2$ and $q^2/\overline{w'^2}$ changes little from its measured value in neutral conditions (which is about 5.5), this expression predicts that $K_\mathrm{H}/K_\mathrm{M}\to 0$ when $Rf=Rf_\mathrm{crit}=0.15$. Again this is much smaller than unity, in agreement with the view that the mixing rate is greatly altered before buoyancy forces have much effect on the overall energy balance (since only the vertical velocity component is directly affected). Equation (5.2.23) can also be regarded as a relation between $K_\mathrm{H}/K_\mathrm{M}$ and Ri; and it is clear that according to this theory the low limit to Rf puts no similar restriction on Ri, which may become large provided $K_\mathrm{H}/K_\mathrm{M}\to 0$.

A second important consequence of Ellison's assumptions is that

$$\frac{(\overline{w'\rho'})^2}{\overline{\rho'^2}\,\overline{w'^2}}=\frac{1-Rf\left[1+\dfrac{q^2}{\overline{w'^2}}\dfrac{T_1}{T_2}\right]}{(T_1/T_3)(1-Rf)} \tag{5.2.24}$$

which decreases towards zero in very stable conditions, instead of remaining constant as Townsend supposed. This shows that

inefficiency of the density transport is due not to the suppression of the velocity and density fluctuations themselves, but to a reduction of the mean product $\overline{w'\rho'}$. (In the limit of pure internal wave motions, ρ' and w' are 90° out of phase, so this correlation tends to zero. See §2.2.1.)

The later theory of Monin (1965) applied a related but more detailed scheme of simplifications to the dynamical equations for all the second moments of the four variables u', v', w' and ρ', instead of just the three considered above. Ellison (1966) (quoted by Yaglom 1969), showed how the resulting system of algebraic equations can be solved to give each of the quantities of interest as a function of Rf. The numerical values of five dimensionless characteristics of turbulence in a fluid of constant density now need to be specified, instead of just the two that were required in (5.2.23). With these stronger constraints, not only does Rf have a critical value, but so does K_H/K_M, the limiting values predicted by Ellison in very stable conditions being $Rf = 0.15$ and $K_H/K_M = 0.5$.

In the following section, experimental and observational results are presented which give support to each of the above conclusions but in rather different circumstances. A critical value of K_H/K_M (and hence of the gradient Richardson number Ri) applies in wake-like flows, which are maintained by Reynolds stresses generated at the edge of the flow itself; once these stresses have become small there is no mechanism for the further generation of turbulent energy (cf. fig. 4.19*b*). Ellison's (1957) theory, which suggests that Ri is unlimited, seems to describe flows over a solid boundary which approximate to the assumed constant-flux layer, and into which there is a continuing supply of turbulent energy (cases (*a*) and (*g*) of fig. 4.19). For this to be possible the relations (5.2.23) and (5.2.24) must be taken to apply to flows which are only intermittently turbulent (§5.1.4), so that the gradients entering into the definitions of Ri are time averaged values, not instantaneous local gradients. This is not inconsistent with the weaker assumptions used by Ellison (1957), whereas the later theory refers more explicitly to a region of fully turbulent fluid.

5.3. Observations and experiments on stratified shear flows

5.3.1. *The generation and collapse of turbulent wakes*

In §§3.1.4 and 4.3.2 we referred to the drag associated with the separation of the flow behind a blunt obstacle and the formation of a turbulent wake. This flow will now be examined in more detail. We begin with a general description of the structure of the wake as it develops downstream under various conditions, both in a continuously stratified fluid and at the interface between two layers, before making the more detailed comparisons with theory.

Immediately behind a cylinder moving horizontally with high Reynolds number (say greater than 10^3, based on the diameter), and moderate Richardson number (say $Ri^{\frac{1}{2}} = \kappa = 0.4$ in the notation of §3.1.4), the wake in a density gradient behaves much as it does in a uniform fluid. Its thickness increases, a small scale turbulent structure is observed, and the shape of the velocity defect profile is little changed. At about ten diameters downstream, however, the rate of growth is clearly being affected, and shortly afterwards the wake collapses as the largest turbulent eddies are rather abruptly suppressed by the stratification. Later the small scale turbulence is also damped out, and the residual motion 100 diameters downstream consists almost entirely of larger scale periodic motions, i.e. of internal waves. This behaviour is illustrated in fig. 5.10 pl. XIII by a sequence of shadowgraph pictures due to Pao (1968*b*). This author has also studied the whole range of wake effects from slow viscous flows (§3.3.3) to the fully turbulent wakes of interest here. At intermediate Reynolds numbers regular vortex shedding can occur as in a uniform fluid, but with stratification the vortices are flattened, and they also act independently to generate internal waves. Such vortices are quite distinct from the rotors which are produced by local overturning of the stratification (by large amplitude lee waves), in regions remote from the obstacle (see §4.3).

Schooley and Stewart (1963) carried out experiments (on a three-dimensional wake behind a self-propelled body) in which they paid special attention to the mechanism of wave generation. They pointed out that the collapsing motion is of just the right kind to generate gravity waves efficiently; it too is driven by gravity, and

must take place at a rate comparable with the vertical velocity in internal waves. An experiment of Wu (1969), in which he studied the collapse of a semi-cylindrical region of uniform fluid in a density gradient, is also relevant here (though there was no small scale turbulence present initially and the later stages of flow, an advancing nose like a gravity current (§3.2.5) and finally a viscously dominated motion (cf. §3.3.4), do not concern us here). He showed that waves are generated which propagate ahead of the advancing front with an initial peak in the energy density at an angle of about 55° to the horizontal (corresponding to a frequency of 0.8 of the buoyancy frequency, §2.2.2). At later times the line of the crests moves toward the horizontal.

The turbulent wake produced by a flat plate towed normal to its plane along an interface between uniform layers of fresh and salt water has been studied more quantitatively by Prych, Harty and Kennedy (1964). Density profiles were measured by withdrawing samples from a rake of probes mounted at various distances behind the plate (and moving with it). Velocity profiles were obtained similarly using a propeller type velocity meter, mostly in a uniform fluid but also, for comparison, in the stratified cases. The measured velocities were in good agreement with a theory which allowed for a backflow arising because of the finite length (10 m) of the tank; the more accurate results for the uniform fluid will be used in the later quantitative calculations. The drag force was also measured directly in all runs. The drag coefficient C_D (defined as in §3.1) changed little with density difference from its value of nearly two in a uniform fluid, so that form drag and not wave drag dominated the behaviour at low *Ri* and high *Re* in these two-layer experiments. (Contrast this with the results for a continuously stratified fluid described at the end of §3.1.4, where both contributions to the drag were seen to be significant.)

The strong effect of stratification on the mixing is clearly shown in the density profiles. Prych *et al.* expressed their results in terms of the parameter

$$J^2 = g\frac{\Delta\rho}{\rho}b_0 \Big/ C_D U^2 \qquad (5.3.1)$$

a kind of overall Richardson number based on the half-width b_0 of the plate and its velocity, but with the drag coefficient added (this

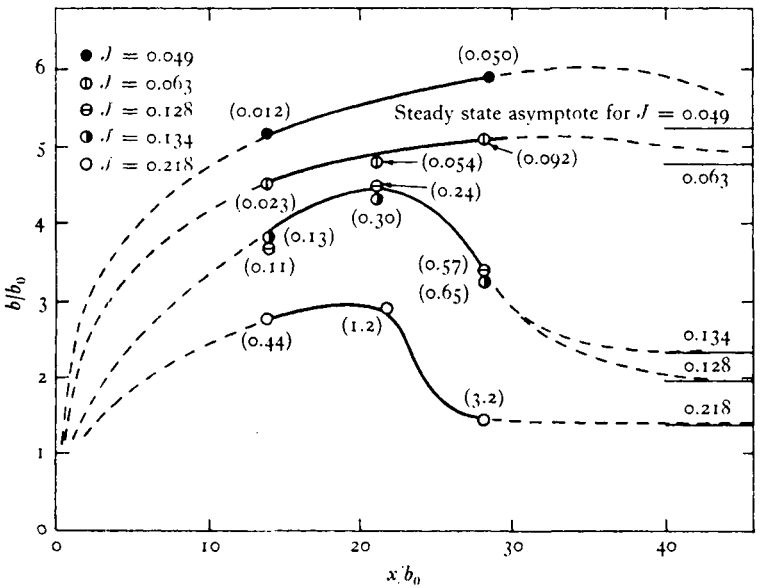

Fig. 5.11. Variation of the width of a wake with distance x behind a plate (of width $2b_0$) towed along an interface between two layers of different density. Curves are shown for various values of the parameter J, and the numbers in brackets are minimum gradient Richardson numbers computed using the data given by Prych, Harty and Kennedy (1964).

enters into their estimate of the work done by the body on the fluid). Numerically, J is very nearly equal to the parameter κ defined in §3.1.4. The rate of spread, and the extent of the later collapse, depend systematically on J as shown in dimensionless form in fig. 5.11, where the separation between two arbitrarily chosen concentrations is plotted against distance downstream.

An overshoot and strong collapse are prominent at the higher values of J. A visual examination of the wake, with one layer dyed, showed that this is the result of large globules of fluid being transferred across the interface by vortices shed by the plate. If the turbulence is damped before much mixing has taken place (as it is when J is large), these settle back to an equilibrium position much closer to the centre of the wake; the final equilibrium thicknesses are shown on the right of fig. 5.11. It is also worth remarking that the final density profile is not far from linear across the centre

of the tank. Stirring in this apparently crude way is a surprisingly effective way of producing a uniform gradient over nearly the whole depth.

5.3.2. *The suppression of turbulence at an interior shear layer*

As our first test of Townsend's predictions (§ 5.2.3) we will use the data just described. There is some uncertainty in the interpretation for developing flows, since a failure of the regulating mechanism of the turbulence does not cause mixing to stop instantly; nevertheless one can deduce a range of conditions over which buoyancy effects are becoming significant.

Minimum gradient Richardson numbers, computed using the (nearly linear) density profiles and the maximum gradients on the corresponding velocity profiles, have been added (in brackets) to the experimental points shown in fig. 5.11. Consider first the experiments with $J = 0.128$, 0.134 (which incidentally give good support to the choice of J as a modelling parameter, since they were carried out with both the density difference and velocity varied). At the position of maximum width the turbulence must already have been strongly affected since the wake collapsed so strongly after this point; thus the values 0.24 and 0.30 are certainly larger than the Ri_{crit} defined in Townsend's sense. The results at lower values of J, which approach their asymptotic values more smoothly, suggest that Ri_{crit} is less than 0.1 and may be as low as 0.05.

Townsend (1957) made similar deductions from observations of a jet of fluid of intermediate density injected along an interface. A complication here was the more rapid spread horizontally than vertically, but he was able to show that mixing of outside fluid into the jet had almost ceased at $Ri = 0.3$. The first signs of an effect of the density gradient on the jet development occurred at about $Ri = 0.05$; the 'critical' value must lie between these extremes, and is probably less than 0.1.

Further examples of the same turbulence suppression mechanism are to be found in flows where the density distribution is stabilizing over a limited range of heights. This often occurs near a boundary, and though superficially the flow then seems more like the cases considered in the following section, the distinguishing feature of

'interior' layers is that the turbulence must be generated elsewhere in the flow, not directly by the shear at the adjacent wall. The laboratory experiment of Nichol (1970) is related to Reichardt's investigation of the stability of a boundary layer under the heated roof of a wind tunnel (discussed in §4.2.2). Instead of heating the whole roof, however, Nichol began heating at some point downstream, and examined the effect of the growing temperature boundary layer on an established turbulent wall layer. He observed a sudden and nearly complete collapse of the turbulence near the wall at some distance behind the leading edge of the heated section, measuring very small values of turbulent intensity and wall stress, and a highly inflected velocity profile with low velocities near the wall. The inside of the wall layer is disconnected from its energy source, though dissipation must still occur near the wall. Townsend (1957) used Nichol's (then unpublished) profiles to give further support to the view that Ri just before collapse is less than 0.1.

A natural example of this phenomenon is the 'dying away' of the wind at night, or more spectacularly, the sudden calm which has been observed during an eclipse of the sun (Townsend 1967). Clearly only the wind near the ground can be changed, since the duration of an eclipse is too short for the geostrophic flow at great heights to be affected, and the wind can remain strong even at tree-top height. When the solar heating is removed, the ground cools by radiation and heat is transferred downwards out of the air towards the ground. This produces a layer with a stable density gradient, whereas previously the whole profile was convectively unstable. As the depth of the stable layer grows, its top reaches a height where the velocity gradient is small, while the density gradient there changes only slowly with the depth. Eventually the value of Ri rises to a value of about 0.1 and the turbulence will die away. (Radiation effects will change the critical value somewhat, but the principle of the argument remains unchanged.) Without any turbulent Reynolds stress, the motion higher up (which has been driving the whole flow) cannot any longer affect the air below, and so the friction at the ground will cause the wind to die away at low levels. (An associated change in the intensity of temperature fluctuations has been documented by Okamoto and Webb (1970).) In time, however, this layer can be accelerated by the overall pressure gradient, and may again

become turbulent for a short while during the night – until the same process begins again and the wind dies down a second time.

The last result recalls again the observations referred to in passing in §4.1.4. Mittendorf (1961) showed that, after the Kelvin–Helmholtz mechanism had led to the breakdown of an interface between two accelerating layers in an inclined tube, the turbulence in the mixing region was suppressed before the transition layer had spread out very far. In one experiment he observed three successive breakdowns of the interfacial region, separated by quiescent periods. While turbulence is present the drag on the layers increases and the velocity falls, but when it is suppressed the flow is accelerated again by gravity. This behaviour can now be interpreted in terms of an increase of an appropriate Richardson number to a stable value, because of the decrease of the velocity gradient due to mixing. In §10.2.3 it will be shown that the supply of energy to the turbulent interface will be cut off when an overall Richardson number based on its thickness reaches a value of order one. During the whole of the thickening process, however, the gradient Ri can be much smaller, allowing turbulence to persist according to Townsend's criterion. (Compare with §6.2.4.)

Finally, it is convenient to mention here a contrasting (but related) natural phenomenon, the wind-driven layer at the surface of the sea. In conditions of strong surface heating, a well-mixed warmer (and therefore lighter) layer is formed, which is of limited depth because the stabilizing density distribution inhibits vertical mixing with the deeper water. (See §9.2.1 for a fuller discussion of the mixing problem.) At the bottom of this surface layer is a strong density gradient where (according to the ideas developed in this section) the turbulence is suppressed and the Reynolds stresses are small. A given wind stress at the surface can thus accelerate the water to produce stronger surface currents in this case compared to the unstratified ocean for two reasons: the depth of the layer involved is smaller, and the retarding stress below it is reduced. The recognition of conditions likely to produce such a 'slippery sea' played a large part in the success of the winning Olympic sailing team at Acapulco in 1968 (Houghton and Woods 1969). (We should however, not forget the 'dead water' effect described in §2.1.2,

which could slow a ship down because of the extra wave drag generated at the interface.)

5.3.3. *Stratified flows in pipes, channels and estuaries*

The flow just discussed also has much in common with those lying at one extreme of the range of enclosed flows to be considered next. Another example is a turbulent layer of salt water flowing under a deep layer of fresh water in conditions where the bottom stress is much greater than that at the interface (which is so when a shallow layer flows along a horizontal bed – see §6.2.3). The intrusion of a saline wedge into an estuary against a fresh water flow (§3.2.5) is also of this kind. The distinguishing feature is that buoyancy effects become dominant somewhere in the interior of the channel, and mixing generated by the shear at the boundary is almost entirely suppressed across a sharp interface bounding one or more well-mixed layers (cf. case (*d*) fig. 4.19).

At the other extreme, the turbulence generated at the boundaries can be so strong that the fluid is thoroughly mixed over the whole depth of the flow (fig. 4.19*a*). This too occurs in natural estuaries, when the tidal current is much larger than the river flow; the salinity is then nearly constant at any section, but decreases gradually with distance upstream. For intermediate conditions, and especially near the turn of the tide, there is a measurable vertical gradient as well as a horizontal one, and the density gradients are clearly having an effect on both the rate of vertical mixing and the longitudinal motion and diffusion.

It was in an 'intermediate' type of flow that the often quoted measurements of velocity and density profiles were made in a tidal channel (the Kattegat) by Jacobson. Taylor's (1931*b*) analysis of these results showed that vertical mixing (at much greater than molecular rates), can persist at time-averaged 'gradient' Richardson numbers (based on measurements made $2\frac{1}{2}$ m apart) of ten or more. The ratio of eddy diffusivities for salt and momentum K_S/K_M deduced from several sections was about 0.03, so that Rf was still less than unity and there was no violation of the energy condition. The discussion given in §5.1.4 suggests however, that such an interpretation is consistent only if the turbulence is very inter-

mittent, not continuous throughout the fluid (case (*g*), fig. 4.19). The stress at the boundary remains an important parameter governing the whole flow, but a large fraction of the momentum flux will be carried by internal waves. (See also § 10.2.)

The whole range of steady two-dimensional pipe or channel flows can also be characterized in an overall way by two parameters, the slope of the pipe and a 'pipe Richardson number'. The latter is most simply defined by

$$Ri_{\mathrm{p}} = \frac{|\rho_{\mathrm{m}} - \rho_0|}{\rho_0} \frac{gd\cos\theta}{U^2}$$
$$= A\cos\theta/U^3 \qquad (5.3.2)$$

where d is the total depth, U is the mean (discharge) velocity, ρ_{m} is the density when the flow is fully mixed across a section, and ρ_0 is the density of the ambient flow (before any buoyant fluid is added). Thus $A = g(\Delta\rho/\rho)dU$ is the buoyancy flux per unit width, which is constant in many problems of interest.

A related, but at first sight very different parameter used by civil engineers to correlate model experiments and field data, is the *estuary number* E_{s}, defined for a tidal channel to be

$$E_{\mathrm{s}} = P_{\mathrm{t}} F_0^2 / Q_f T. \qquad (5.3.3)$$

Here P_{t} is the 'tidal prism' (the volume of sea water entering the estuary on the flood tide), $F_0 = U/(gd)^{\frac{1}{2}}$ is an ordinary Froude number based on the tidal mean velocity and the depth, Q_f is the fresh water discharge and T the tidal period. (See for example Harleman and Ippen (1967).) From its definition, $P_{\mathrm{t}} = UbdT$, where b is the width of the estuary, so that

$$E_{\mathrm{s}} = \frac{P_{\mathrm{t}} U^2}{gdQ_f T} = \frac{U^3 b}{gQ_f}. \qquad (5.3.4)$$

Writing $A = g(\Delta\rho/\rho)Q_f/b$ and comparing (5.3.2) and (5.3.4) gives finally

$$Ri_{\mathrm{p}} = E_{\mathrm{s}}^{-1} \frac{\Delta\rho}{\rho}. \qquad (5.3.5)$$

The density ratio factor is a constant for a particular estuary (and about 0.02 for all estuaries), so Ri_{p} and E_{s} are just inversely related. According to Harleman and Ippen, the division between 'stratified'

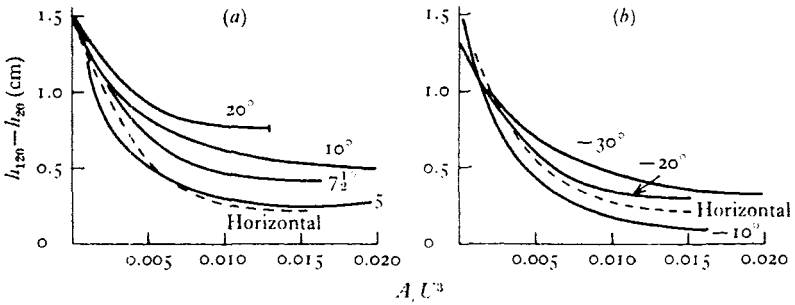

Fig. 5.12. Mean experimental curves showing the increase in thickness of a layer of salt solution as it flows between two sections 1 m apart under an uphill flow of fresh water. (*a*) Fully reversed layer. (*b*) Layer flowing downhill, with gravity but against the main flow. (From Ellison and Turner 1960.)

and 'well-mixed' cases occurs in the range $E_s = 0.03$–0.3, increasing values corresponding to increasingly mixed conditions.

The laboratory experiments of Ellison and Turner (1960) support this choice of overall governing parameters. They measured the rate of spread of a layer of salt solution, injected into the bottom of an inclined pipe of rectangular section through which there was a steady turbulent flow of fresh water. When the pipe was horizontal or the flow was downhill, the mixing rate was small, and when the flow was uphill two cases were distinguished. At low 'ventilating' velocities a thin layer of salt solution crept back along the pipe against the main flow, but at higher flow velocities all the salt was immediately carried uphill, in a layer which thickened with distance. (The criterion for reversal is discussed in §6.2.) As shown in fig. 5.12, the increase of depth of the salt layer in the 'fully reversed' cases depends systematically on θ and Ri_p, with quite a strong dependence on slope. At low values of Ri_p all curves come together, as they must when density differences are negligible. Buoyancy effects are already important at $Ri_p = 0.005$, by which time the rate of spread at small slopes has decreased by a factor of three.

Bakke and Leach (1965) have applied the results of these and similar experiments to describe the behaviour of layers of methane gas flowing along the roof of a coal mine. They defined a 'layering number', equivalent to $Ri_p^{-\frac{1}{3}}$ in the notation of (5.3.2), and were able

to recommend minimum values of this parameter for various slopes, such that explosive concentrations of gas will be confined to acceptably short sections of a mine. This application is discussed further in §6.2.3.

We now turn to an interpretation of the same laboratory experiments in terms of the detailed local properties, which led to a test of Ellison's (1957) theory. Ellison and Turner (1960) showed that the distortion of the velocity profile in a tilted pipe depends mostly on Ri_p. Choosing cases where the profile changed least with distance, and combining the velocity measurements with salinity profiles at two sections, they were able to estimate K_S and K_M for salt and momentum, as a function of position in the flow and over a range of stability condition. A consistent correlation with local values of Ri were obtained at two heights intermediate between the wall and the centre of the channel, where the salt flux and Ri were changing least rapidly. K_M is affected rather little by the density gradient, whereas K_S/K_M is a strong function of Ri, as shown in fig. 5.13. It is by no means obvious that such a dependence on a strictly local parameter should emerge under the conditions of this experiment, when Ri is varying and the turbulent eddies cover a considerable range of heights. (Refer to the discussion on p. 150.)

On fig. 5.13, which is plotted using a logarithmic scale to cover a large range of Ri, is also shown the family of theoretical curves predicted using (5.2.23). The form of each of these is fixed once one specifies the value of Rf_{crit} and $b = 1.4$, the measured value of K_H/K_M (or of K_S/K_M, since no molecular effects are taken into account here) in neutral conditions. The experimental points are best fitted by the curve corresponding to $Rf_{crit} = 0.15$, in agreement with the estimate made earlier on purely theoretical grounds. At higher Ri, the theoretical curves are also broadly in agreement with Taylor's values (mentioned above) but the comparison is less sensitive in this range as well as the theory being more questionable.

A related experiment using air as the working fluid was carried out by Webster (1964). He investigated the detailed structure of a turbulent stratified shear flow, using a specially designed wind tunnel with differential heating to produce the density gradient, and comparing his results with the theories of Ellison and Townsend. He showed that various fluctuating quantities such as the mean

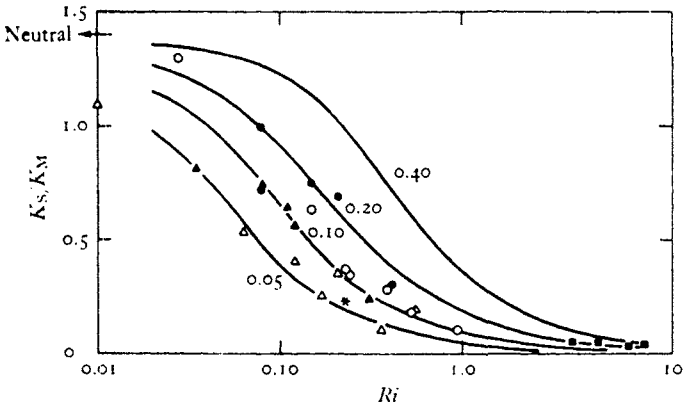

Fig. 5.13. Ratio of the transport coefficients for salt and momentum plotted against Richardson numbers deduced from time-averaged profiles, on a logarithmic scale. Various laboratory measurements reported by Ellison and Turner (1960) are compared with the theory of Ellison (1957); values of Rf_{crit} are marked on the theoretical curves. The Kattegat results, as analysed by Taylor (1931*b*), are also plotted as the squares on the far right of the diagram.

square temperature fluctuation (normalized with the local temperature gradient) and the ratio of the turbulent transports of heat in the downstream and vertical directions, as well as the ratios K_H/K_M deduced from correlation measurements, depend systematically on Ri. The trend of decreasing K_H/K_M with increasing stability was confirmed, and the existence of a critical value of Rf supported, but the absolute values were high compared with other experiments (even in near-neutral conditions). The discrepancy can be attributed to the development of the flow, which probably never reached equilibrium and still depended strongly on the properties of the decaying wakes behind the grid bars which produced the shear. A much larger wind tunnel is needed to remove these ambiguities; recent developments in this field have been reported by Arya (1972).

5.3.4. *Longitudinal mixing and advection*

Another important property of the estuary flows described above is the longitudinal spread of the region of mixing between the fresh and salt water. When an estuary is not far from the well-mixed state, and the fresh water flow is constant, the transition region can be

described reasonably well using a one-dimensional diffusion equation, with a longitudinal dispersion coefficient which is determined by the mean flow over a long time. The shape of the salinity distribution changes little in one tidal cycle, but just shifts back and forth between low and high tide marks; the fresh water flow may however change relatively rapidly, and this can give rise to difficulties in evaluating the dispersion coefficient from observations. (See Ward and Fischer 1971.) The model can be adapted to include flows having considerable vertical salinity gradients, provided the diffusivity (and certain other parameters specifying the boundary conditions) are allowed to be empirical functions of E_s defined by (5·3·3).

Physically it is clear that a strictly one-dimensional model is an oversimplification. Firstly, the motions arising because the fresh water tends to flow on top of the salt must play a role in any channel which is not perfectly mixed. When this density driven flow is accompanied or followed by vertical mixing, the result is an apparent increase in the 'longitudinal diffusivity'. The longitudinal spread will be largest when the rate of vertical mixing is small, since then the shear will have its maximum effect. (Compare this with the result of Taylor (1954), who showed how the non-uniform velocity profile enhances the longitudinal spread in a turbulent pipe flow.) Secondly, Fischer (1972) has shown that the non-uniformity of the velocity in the lateral directions, due to variations in depth, can have an even larger effect on longitudinal dispersion than do the vertical shears. The combination of small scale, vertically controlled mixing with the mean horizontal shear is very effective because the widths of estuaries are usually so much larger than their depths.

An experiment which isolates the effect of the density-driven flow from that of the tidal motion has been performed by Harleman, Jordan and Lin (1959). They stirred mechanically over the whole length and depth of a large laboratory tank (to simulate mixing due to many tidal excursions), and measured the horizontal concentration profiles as a function of time after a central barrier separating fluid of different densities had been removed. With no density difference the effective diffusivity K was approximately proportional to the stirring velocity. When the density difference was 1 %, the diffusivity (K' say) was the same as K at high stirring rates, but

$K' - K$ was inversely proportional to turbulent intensity over the range of conditions they studied.

Most attempts at solving even a fully two-dimensional problem have fallen short of being complete theories, but they can nevertheless provide a useful framework for the comparison of observations and for the evaluation of the dependence of vertical and longitudinal diffusivities on other parameters. A notable contribution is that of Hansen and Rattray (1965), who surveyed the previous work and themselves gave solutions which cover a wide range of observed types of flow in an estuary. Using equations derived by averaging over a tidal cycle, they distinguished modes of motion associated with the mean fresh water flow, the differential motion due to density gradients (and a third caused by surface wind stress, which will not be discussed further here). Note that nearly uniform salinity in the vertical does *not* imply the absence of gravitational effects; especially in deep channels there can be a reversal of mean longitudinal velocity with depth even with only slight stratification. (See also Abbott 1960.)

Finally, it is instructive to present in this context the similarity solution used by Phillips (1966*b*) to describe the buoyancy-driven circulation in an almost enclosed sea, such as the Red Sea. There are some important differences and simplifications here: the flow can be regarded as steady, and both the longitudinal density differences driving it and the turbulent stirring are produced in another way, by surface cooling and evaporation. If there is a sill (of depth d) far from the origin, the flow has the form shown in fig. 5.14, inwards at the surface and out again below, with little motion below the sill depth. The surface density must increase with distance from the entrance, while the density profiles must remain stable throughout.

The only external parameters defining the flow are the length-scales x and d and the downward buoyancy flux B defined by (5.1.7), which is assumed independent of position. The expression of B in terms of the sensible heat flux H must now, however, be modified to take into account density changes produced by the increase of salinity S due to an evaporation rate E, i.e.

$$B = \frac{-g}{\bar{\rho}} \left[(H - LE) \frac{\alpha}{C_p} - ES \right], \tag{5.3.6}$$

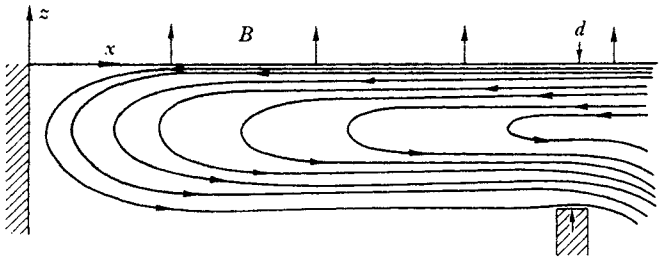

Fig. 5.14. Sketch of the streamlines in a convective motion driven by a uniform surface buoyancy flux, with a sill of depth d far from a vertical boundary at $x = 0$. (From Phillips 1966*b*.)

where L is the latent heat and α the coefficient of expansion. Using dimensional reasoning with the constraints imposed by the governing equations, Phillips showed that the longitudinal velocity and the density distribution must have the forms

$$U = (Bx)^{\frac{1}{3}} f\left(\frac{z}{d}\right), \tag{5.3.7}$$

$$g\frac{\rho'}{\bar{\rho}} = B^{\frac{2}{3}} x^{\frac{2}{3}} d^{-1} j\left(\frac{z}{d}\right). \tag{5.3.8}$$

(Compare these with (5.2.2) and (5.2.3); dimensionally the arguments are closely related.) There are no current data which allow (5.3.7) to be tested, but measurements of the longitudinal density variations in the Red Sea agree with the $\frac{2}{3}$ power law predicted by (5.3.8). Vertical buoyancy profiles scaled in this way all fall close to a single curve, giving further strong support to the solution and permitting the empirical evaluation of the dimensionless function j.

We should also note that in this kind of turbulent convective motion the turbulence adjusts itself so that there is everywhere a balance between the mean shear, the buoyancy and the Reynolds stress terms: all are of the same order of magnitude. It follows from (5.3.7) and (5.3.8) that the mean gradient Ri must be independent of B and x (but it may still be a function of z/d), and the same is true of Rf. In view of the prediction made in (5.1.23), one can speculate that the case considered here is another kind of internally determined flow, for which there will be unique constant values of Ri and Rf (or K_ρ/K_M).